# Sustained Microglial Activation in the Area Postrema of Collagen-induced Arthritis Mice: a Potential Pathway Linking Arthritis and the Brain

**Takayuki Matsushita** ( h20ms-matsushita@jikei.ac.jp )
Jikei University School of Medicine: Tokyo Jikeikai Ika Daigaku https://orcid.org/0000-0002-1297-6137

**Kazuhiro Otani**
Jikei University School of Medicine: Tokyo Jikeikai Ika Daigaku

**Yohsuke Oto**
Jikei University School of Medicine: Tokyo Jikeikai Ika Daigaku

**Yukari Takahashi**
Jikei University School of Medicine: Tokyo Jikeikai Ika Daigaku

**Daitaro Kurosaka**
Jikei University School of Medicine: Tokyo Jikeikai Ika Daigaku

**Fusao Kato**
Jikei University School of Medicine: Tokyo Jikeikai Ika Daigaku

**Research article**

**Keywords:** central nervous system, circumventricular organs, area postrema, microglia, interleukin-1β, collagen-induced arthritis, rheumatoid arthritis

**Posted Date:** March 26th, 2021

**DOI:** https://doi.org/10.21203/rs.3.rs-361550/v1

# Abstract

**Background.** Neuropsychological symptoms are common complications among patients with rheumatoid arthritis (RA), while it is largely unexplored how RA pathology spread to brain protected by blood-brain barrier (BBB). The sensory circumventricular organs (sCVOs) (brain regions lacking a blood–brain barrier) is the brain site that peripheral inflammatory signals, such as blood cytokines and chemokines, can directly access and modulate cell activities in the brain parenchyma. To determine whether microglia, resident immune cells in neuronal tissue, in the sCVOs can function as an interface between peripheral inflammation and brain under the autoimmune-arthritis conditions, we analyzed microglia in the sCVOs of a mouse model of collagen-induced arthritis (CIA).

**Methods.** Microglial number and morphology were analyzed in the sCVOs of CIA and control mice (controls were administrated Freund's adjuvant [FA] and/or saline). Immunostaining for ionized calcium-binding adaptor molecule-1 was performed at various disease phases: "pre-onset" (post-immunization day [PID] 21), "establishment" (PID 35), and "chronic" (PID 56 and 84). Quantitative analyses on microglial number and morphology were performed, with principal component analysis used to classify microglia. Interleukin-1β (*IL-1β*) mRNA expression in microglia was also analyzed by multiple fluorescent *in situ* hybridization.

**Results.** In the area postrema (AP), one of the sCVOs located in the medulla, microglia significantly increased in density (CIA, $n = 15$; FA, $n = 6$; saline: $n = 10$) with changes in morphology during the establishment and chronic phases. In other sCVOs (subfornical organs [SFO] and organum vasculosum laminae terminalis [OVLT]), microglial changes were not significant. In the AP microglia, non-subjective clustering classification of cell morphology (CIA, 1,256 cells; saline, 852 cells) showed that the proportion of microglia in a highly activated form was increased in the CIA group. Also, the density of *IL-1β*-positive microglia, a hallmark of functional activation, increased in the AP. These microglial changes in the AP persisted until the chronic phase.

**Conclusions.** Our findings indicate that an increase and activation of microglia is sustained in the AP during chronic arthritis. This suggests that there is a direct physiological pathway linking peripheral arthritis to the brain through the AP.


# Background

Neuropsychological symptoms, such as hyperalgesia, cognitive dysfunction, depression, and fatigue are common complications among patients with rheumatoid arthritis (RA) (1–4). These symptoms lead to a reduced quality of life, lower rate of disease improvement, and poorer life prognosis (5–7), and are associated with elevated annual healthcare costs (8). To ameliorate these neuropsychological complications of RA, it is necessary to understand the underlying mechanisms within the central nervous system (CNS) of patients with RA. Despite recent advances in functional brain imaging technologies,

which have shown aberrant brain activities in patients with RA (9), how peripheral events in RA affect brain function remains largely unexplored.

The sensory circumventricular organs (sCVOs), subfornical organs (SFO), organum vasculosum laminae terminalis (OVLT), and area postrema (AP), are sites of potential periphery-to-brain channels. The sCVOs have weaker blood–brain barrier (BBB) function with highly-permeable fenestrated capillaries, which allows molecules involved in RA pathology to penetrate neural tissue and directly affect nervous system function (10). Indeed, the sCVOs express receptors for cytokines (namely, interleukin [IL]-1 receptor, IL-6 receptor, tumor necrosis factor [TNF] receptor, and interferon-gamma [IFN-γ] receptor) (11–14) and chemokines (namely, chemokine receptor type 5 and prokineticin receptor 2) (15,16). Systemic activation of these receptors by exogenous cytokines leads to expression of downstream signaling within the sCVOs (17,18). Following systemic administration of IL-1β in rats, the number of neurons expressing c-Fos (a marker of neuronal activity) in the hypothalamus is increased, as are plasma adrenocorticotropic hormone levels, in a manner that is dependent on an intact AP (19). These findings suggest that serum cytokines can directly affect brain function via the sCVOs.

The sCVOs are also known for their rich presence of microglia (20), the resident immune cells of the CNS, which continuously survey the local brain environment (21). Pathological conditions such as brain injury, infection, and neurodegeneration, increase the number of microglia cells and transform their morphology. Morphologically activated microglia are characterized by an ameboid-shape with a swollen cell body (22), and also by expression and release of inflammatory cytokines (23) that can modulate neuronal activity (24), which suggests their morpho-functional coactivation (25). It is likely that microglia in the sCVOs play a role in mediating peripheral inflammation and neuronal activity in the brain, as shown in various inflammatory disease models, such as bleomycin-induced lung injury and dextran sulfate sodium induced colitis (26,27). We therefore determined whether microglia in sCVOs are morpho-functionally activated in collagen-induced arthritis (CIA) mice, a model for RA with autoimmune arthritis and increased levels of systemic inflammatory mediators (28) that can activate microglia cells (29–31). Here, we show that microglia in the AP of CIA mice remain activated during the prolonged course of arthritis progression.

## Methods

# Animals

Male DBA/1J mice were purchased from Sankyo Labo Service (Tokyo, Japan). They were housed in groups of 4 to 6 and maintained on a light/dark cycle of 12:12 hours with food and water available ad libitum.

# Detecting the circumventricular organs using fluorescein isothiocyanate

To visualize the sCVOs of DBA/1J mice, the fluorescein isothiocyanate (FITC) method was used according to a previous report (32). Briefly, 12-week-old mice were anesthetized using isoflurane (3% in 100% $O_2$) and transcardially perfused with the following: first, 0.1 M phosphate-buffered saline (PBS), 5 ml; second, FITC in PBS (0.1 mg/ml), 25 ml; third, PBS, 12.5 ml; and finally, 4% paraformaldehyde (PFA) in 0.1 M phosphate buffer (PB), 40 ml. Dissected brains were postfixed overnight and cryo-protected. Brain blocks were embedded in OCT Compound (Sakura Finetek, Tokyo, Japan) and stored at −80°C. Consecutive coronal sections (20 μm) were obtained throughout brain regions containing the third ventricle and medulla using a cryostat (CM1850; Leica Biosystems, Tokyo, Japan). Every second section was embedded in anti-fading Aqua Poly/Mount (18606; Polysciences, Warrington, PA, USA) onto coverslips.

# Collagen-induced arthritis

After acclimation for 1 week, 7-week-old mice were used. According to a previous report, the immunization procedure comprised two intradermal injections at the base of the tail on post-immunization days (PID) 0 and 21 (33,34). In the CIA group ($n$ = 99), a first immunization of bovine type II collagen (200 μg/mouse; Collagen Research Center, Tokyo, Japan) dissolved in 0.1 M acetic acid (4 mg/mL) emulsified in complete Freund's adjuvant (CFA; Becton Dickinson and Company, Franklin Lakes, NJ, USA) was administered on PID 0, with a booster immunization of bovine type II collagen dissolved in 0.1 M acetic acid emulsified in incomplete Freund's adjuvant (IFA; Becton Dickinson and Company). In the Freund's adjuvant group (FA group; $n$ = 12), 0.1 M acetic acid without type II collagen emulsified in CFA (PID 0) and IFA (PID 21) were administered in the same manner. In the saline group ($n$ = 52), an equivalent volume of saline was administered. Immunization was performed in a blinded fashion in the CIA and FA groups, but not the saline group, because of differences in appearance of the saline and emulsions. According to a previous report, arthritis severity was determined using arthritis scores for all four limbs on the following scale: 0, normal; 1, swelling of digits alone or localized swelling of wrist and ankle joints; 2, swelling of both digits and wrist or ankle joints; and 3, swelling of a whole limb (34). "Total arthritis score" defined the sum of the scores for all four limbs. Brain analyses (described below) were performed on PID 21 and 35 and considered to represent the pre-onset and establishment phases, respectively, while those on PID 56 and 84 represented chronic phases. Several mice with ulceration around the anus caused by CFA (CIA, 6 of 99; FA, 1 of 12) were excluded from further analyses. Finally, 93 CIA mice, 11 FA mice, and 52 saline mice were used in this study.

# Tissue preparation

For immunohistochemistry, mice under anesthesia were transcardially perfused with PBS followed by 4% PFA in 0.1 M PB. After post-fixation, the brain was cryo-protected. Brain blocks were embedded in OCT compound and stored at −80°C. Sections containing the SFO, OVLT, or AP were obtained using a cryostat at a thickness of 20 μm. For *in situ* hybridization, mice under anesthesia were transcardially perfused

with PBS. The unfixed medulla was dissected and frozen in isopentane on dry ice, and 16 μm coronal sections were obtained using a cryostat.

# Immunohistochemistry

Sections were washed in PBS and then incubated in blocking solution containing 1% bovine serum albumin and 0.3% Triton X-100 in PBS for 1 h at room temperature. Subsequently, sections were incubated for 21 h at 4°C with rabbit anti-mouse ionized calcium-binding adaptor molecule-1 (Iba-1) (1:4000; Wako Chemicals, Osaka, Japan), mouse anti-mouse glial fibrillary acidic protein (GFAP) (1:2000, G3893; Sigma–Aldrich, St. Louis, MO, USA), and/or American-hamster anti-mouse CD31 (1:100, 2HB; Developmental Studies of Hybridoma Bank, Iowa University, Iowa City, IA, USA). After rinsing in PBS, sections were incubated for 2 h at room temperature with the following secondary antibodies: Alexa Fluor 488-conjugated goat anti-mouse IgG (1:1000; Thermo Fisher Scientific, Rockford, IL, USA), Alexa Fluor 568-conjugated goat anti-rabbit IgG (1:1000; Thermo Fisher Scientific), and/or Alexa Fluor 647-conjugated goat anti-American-hamster IgG (1:400; Jackson ImmunoResearch, West Grove, PA, USA). Sections were then washed with PBS and incubated with 4',6-diamidino-2- phenylindole (DAPI) (1 μg/ml; Dojindo, Kumamoto, Japan) for nuclear staining. Slices were embedded in anti-fading Aqua Poly/Mount on coverslips.

# Multiplex fluorescent in situ hybridization

Multiplex fluorescent RNAscope (Advanced Cell Diagnosis [ACD], Hayward, CA, USA; Medical & Biological Laboratories, Nagoya, Japan) was performed using probes for *Iba-1* (Mm-Aif1, #319141) and *IL-1β* (Mm-Il1b-C2, #316891C2), in accordance with the manufacturer's instructions. Briefly, after fixation in 10% neural-buffered formalin at 4°C for 15 min, sections were washed with PBS, incubated in ethanol, and air-dried. Sections were incubated with protease III (diluted 1:1 with PBS) for 30 min. After additional PBS washing, probe hybridization and amplification steps were performed. *Iba-1* (Alexa 488) and *IL-1β* (Atto 550) probe-stained sections were incubated with DAPI and mounted with Aqua Poly/Mount on coverslips.

# Image acquisition

All fluorescence images were obtained using laser scanning confocal microscopy (FV1200; Olympus, Tokyo, Japan). Grayscale (16 bit) images were captured with a c-MOS camera (1024 × 1024 pixels, DP80; Olympus) and saved in TIFF format.

# Quantitative analysis for immunohistochemistry

All image analyses were performed by a blinded examiner using ImageJ (National Institute of Mental Health, Bethesda, MD, USA). Images for Iba-1 immunosignal were captured with a 20× objective lens to

identify microglia cells using the “triangle methods” with the same threshold value for all analyses. The number of microglia was counted using the “analyze particle” function in ImageJ by setting “size (pixel$^2$)” to 75 - infinity and “circularity” to 0.0–1.00. The area for the sCVOs was determined using DAPI staining in each image by identifying areas with high DAPI-positive signal density. After measuring the sCVO area, the ratio of total Iba-1 immunopositive area to sCVO area (in %) and specific number of microglia (in/mm$^2$) were calculated. Values were calculated in duplicate from two sections per animal.

For evaluation of microglial morphology, quantitation was performed on immunostained images using a 40× objective lens. Regions of interest were placed on the four main divisions of the AP based upon GFAP immunostaining, as described previously (Supplementary Figure 1) (10,35). Binary images in each region of interest were acquired using the same threshold algorithm (at least eight regions from two slices per mouse). To extract single cell images, binary images were segmented using the “analyze particle” function by setting “size (pixel$^2$)” as 300-infinity and “circularity” as 0.0–1.00. The following twelve morphological parameters were measured in each cell: perimeter, area, ratio of perimeter to area, ferret length, minimum ferret length, maximum and minimum diameter of approximate ellipse, aspect ratio, (minimum diameter/maximum diameter), ratio of width to height, circularity, roundness, and solidity (Supplementary Figure 2).

# Quantitative analysis for multiplex fluorescent in situ hybridization

A blinded examiner performed the following image analyses. First, using the “max entropy” threshold method in ImageJ, separate binary images were created for each *IL-1β* and *Iba-1* mRNA signals obtained after RNAscope processing. The number of puncta for *IL-1β* and *Iba-1* located within DAPI-positive nuclei within the AP were counted. According to the scoring guideline for RNAscope images provided by ACD, *IL-1β*-positive microglia cells (identified by nuclear *Iba-1* and *IL-1β* mRNA signals *[IL-1β$^+$Iba-1$^+$*DAPI$^+$]) were classified using the following *IL-1β* expression scales: *“IL-1 β$^{neg}$Iba-1$^+$*DAPI$^+$”, no-expression; “*IL-1β$^{low}$Iba-1$^+$*DAPI$^+$”, co-existence of 1–3 nuclear puncta; and “*IL-1β$^{high}$Iba-1$^+$*DAPI$^+$”, co-existence of 4 or more nuclear puncta. Values from two slices from a single mouse were averaged.

# Quantitative real-time polymerase chain reaction

RNA extraction and real-time polymerase chain reaction (PCR) were performed as described previously (34). Briefly, total RNA was extracted from four amputated limbs using a RNeasy Lipid Tissue Mini Kit (Qiagen, Tokyo, Japan). Real-time PCR was performed using an Applied Biosystem StepOnePlus Real-Time PCR System (Thermo Fisher Scientific, Waltham, MA, USA) with Taqman probes and the following primers: *IL-1β* (Mm01336189_m1), *IL-6* (Mm00446190_m1), and *Actb* (Mm00607939_s1). Expression levels normalized to *Actb* were analyzed using the $^{\Delta\Delta}$CT method. mRNA expression levels were represented as values relative to the average of the saline group.

# Statistical analysis

Data were expressed as mean ± SEM. All statistical analyses were performed using R (version 3.6.1; the R foundation for Statistical Computing, Vienna, Austria) and EZR (Saitama Medical Center, Jichi Medical University, Saitama, Japan)(36). Sample sizes for the experiments on PID 21, 56, and 84 were calculated using expected effect size and variance based on data of Iba-1-immuno-stained area (%) in the AP on PID35. The Kolmogorov–Smirnov test was used as a test of normality. Unpaired *t*-test (two-sided) was used for comparison between two groups. When the normal distribution was not confirmed, the Mann–Whitney *U* test was used to compare the mean ranks of two groups. Three groups were compared by one-way analysis of variance (ANOVA) followed by a Bonferroni post-hoc test. Correlation analysis was performed using Spearman's rank correlation. To classify cells according to morphological parameters, principal component analysis (PCA) and hierarchical clustering analysis (HCA) were used. Frequencies of categorical variables were compared using the chi-square test. Differences were considered significant when the *p* value was < 0.05.

## Results

# Microglial changes in sCVOs on PID 35

There are no published reports describing sCVOs in DBA/1J mouse brain. Thus, we first detected the SFO, OVLT, and AP in DBA/1J mice by observing extravascular leakage of FITC at regions lacking a BBB (Supplementary Figure 3) (32,37). On PID 35, immunostaining for Iba-1 was performed in the AP (Figure 1A-1). To determine the influence of arthritis, the saline and FA groups served as controls for the CIA group. Iba-1 immunostained area (%) and number of microglia (/mm$^2$) were significantly increased in the CIA group (Figure 1A-2). There were no significant differences between the saline and FA groups (Figure 1A-2). Therefore, only the saline group was used as a control group for the rest of the AP experiments. We also similarly examined Iba-1 immunostaining in the SFO (Figure 1B) and OVLT (Figure 1C). There were no significant differences between the CIA and FA groups in Iba-1 immunostained area (%) and number of microglia (/mm$^2$) in these regions (Figure 1B-2, 1C-2).

# Microglial changes in the AP over the disease course

We next analyzed microglia from the pre-onset phase (PID 21) to chronic phases (PID 56 and 84) in CIA and saline mice (Figure 2). Gradual increases in Iba-1 immunoreactivity during these phases in both the saline and CIA groups were observed, which might have resulted from non-disease-associated activation of microglia (38). Nevertheless, high-magnification images showed more extensive Iba-1-immunoreactivity in the CIA group compared with the saline group on PID 56 and 84 (Figure 2A, B), in a similar manner to that on PID 35 described above (Figure 1). At these disease phases, Iba-1-immunoreactivity in the CIA group was manifest in swollen cell bodies (Figure 2B).

This sustained, specific pattern of microglia activation was associated with symptoms that developed during the course of arthritis, including joint swellings (arthritis scores) and body weight changes. The joint swellings persisted until PID 56 and 84 (Figure 3A). Body weight changes in the CIA group were significantly lower than in the saline group in these phases (Figure 3A). Likewise, mRNA expression of *IL-1β* and *IL-6* was significantly higher in the joints of all four limbs in the CIA group than the saline group on PID 56 and 84 (Supplementary Figure 4). These findings demonstrate that inflammatory symptoms and biochemical activation persist at the chronic phase, in which microglial activation remained. To quantitatively confirm this association, we performed quantitative analyses of microglia number and density on PID 21, 56, and 84 (Figure 3B). Iba-1 immunostained area (%) and number of microglia (/$mm^2$) were significantly higher in the CIA group than the saline group at PID 56 and 84 (Figure 3B). Neither parameter differed significantly on PID 21, similar to the arthritis symptoms.

# Microglial morphology in the AP in various disease phases

To compare microglial morphology in the CIA and saline groups, morphological parameters of Iba-1 immunostaining in the AP were measured on PID 21, 35, 56, and 84 (Supplementary Figure 2). On PID 21, no parameter showed a significant difference between groups (Supplementary Figure 5). Several parameters differed significantly between groups on PID 35, 56, and 84 (Supplementary Figures 6–8). In particular, a larger perimeter and smaller circularity were both significant in the CIA group on PID 35, 56, and 84. All morphological parameters of 2,118 cells from 51 mice on PID 21, 35, 56, and 84 (CIA, $n$ = 25; saline, $n$ = 26) were subjected to PCA to identify principal components. The first principal component (PC-1) and second principal component (PC-2) accounted for 74.4% of the observed variability (Supplementary Table 1). To classify microglia according to the measured morphological parameters, HCA was performed using PC-1 and PC-2, which automatically divided all microglia into two clusters (Figure 4A). Cluster-1 microglia were characterized by swollen cell bodies, which is one of the characteristics of activated microglia (22), and were identified by a higher perimeter, area, and minor diameter values, and a lower circularity value. Conversely, cluster-2 microglia were characterized by small cell bodies (Figure 4B). The proportion of cluster-1 microglia in the CIA group was significantly larger than the saline group on PID 35, 56, and 84, but not PID 21 (Figure 4C).

# Correlation between number of cluster-1 microglia and body weight changes

We examined correlations between microglia number and total arthritis score and body weight changes on PID 35 (Figure 5). Number of microglia showed no correlation with total arthritis score or body weight changes from PID 0 (Figure 5A, B). However, examining within each cluster, we found that the number of cluster-1 microglia significantly correlated with body weight changes from PID 0 (Figure 5D). Conversely, the number of cluster-2 microglia did not correlate with body weight changes (data not shown). There

were no significant correlations between microglia number in each cluster and total arthritis score (Figure 5C).

# Increase of IL-1β-positive microglia in the AP

IL-1β is one of the molecules produced by activated microglia (23). We performed *in situ* hybridization to detect microglial *IL-1β* mRNA expression in the AP on PID 35. By combining *IL-1β* and *Iba-1* mRNA expression with DAPI staining, co-expression of *IL-1β* and *Iba-1* mRNA was found in the AP (Figure 6A). In the CIA group, there was an increase in co-expressing nuclei, and several nuclei exhibited high-density expression of *IL-1β* mRNA (Figure 6A). Quantitative analysis revealed that the number of co-expressing nuclei (*IL-1β*$^{+}$*Iba-1*$^{+}$DAPI$^{+}$) (i.e., *IL-1β*-positive microglia) was significantly increased in the CIA group (Figure 6B). To quantify microglia with high-density *IL-1β* mRNA, the number of high-*IL-1β* expression nuclei with co-existence *Iba-1* puncta (*IL-1 β*$^{high}$*Iba-1*$^{+}$DAPI$^{+}$) were also counted. Consequently, the proportion of *IL-1β*$^{high}$*Iba-1*$^{+}$ nuclei to *IL-1β*$^{+}$*Iba-1*$^{+}$ nuclei significantly increased in the CIA group compared with the saline group (Figure 6C).

# Discussion

To identify the mechanism underlying the association between RA pathology and neuropsychological complications in patients with RA, we used a mouse CIA model to examine the hypothesis that microglia, the first-line responders in the brain to inflammatory mediators, are activated in brain regions where the inflammatory blood–brain contact is enabled. To do this, we visualized microglia in the sCVOs during progression of CIA and found that the AP, but not SFO and OVLT, present a marked increase in the number of Iba-1-expressing microglia, lasting from onset to chronic phases of CIA. In addition, non-subjective clustering classification of microglia morphology revealed that this increase in number was accompanied by a drastic shift to a form suggestive of microglia activation. In support of this, a proportion of microglia expressing *IL-1β* increased in this establishment phase. Interestingly, this increase in number of activated-form microglia in the AP negatively correlated with body weight changes. Interpretation of these results is discussed below.

Using similar CIA models in mice, recent studies have demonstrated aberrant behavior resulting from functional brain alterations, such as anhedonia and modified environmental preference (33,39). However, it remains unknown how peripheral inflammatory signals affect brain function, and in turn, behavioral outcomes. Our present study is the first to suggest that 1) sCVOs, particularly the AP, might be the site of transmission of inflammatory factors to the brain under CIA conditions because of a weakened BBB function; and 2) microglial cells in the AP might be the intracerebral receptors of inflammatory signals that are translated into activation of these cells. It is unlikely that this microglial activation results from the effect of CFA injected at the first immunization, albeit CFA is a potent pro-inflammatory agent (40), because we found no significant sign of microglia activation in the AP of mice treated with only CFA at PID 35. A plausible scenario is that circulating cytokines and chemokines are increased in the CIA model

in the establishment phase (28) and enter into the AP and directly activate microglia, which have a large variety of receptors for inflammatory mediators (41).

Accumulating evidence indicates that microglial cells, particularly when they are activated, can affect neuronal excitation and synaptic transmission (24,42). AP neurons send axons to the parabrachial nucleus and nucleus of the solitary tract, which in turn affect the activity of higher brain centers, such as the amygdala and hypothalamus. These regions play roles in homeostatic regulation, such as for appetite, nausea, respiration, and cardiovascular control (10). The observed negative correlation between the number of cluster-1 microglia in the AP and body weight changes in the establishment phase is reminiscent of the drastic changes in appetite in animals with systemic inflammation and subsequent microglia activation in the arcuate nucleus, a center controlling feeding behavior (43). In this regard, marked activation of the AP among the sCVOs in CIA mice is interesting because this might explain specific homeostatic outcomes in this model compared with systemic inflammation. The mechanism underlying this AP specificity remains unidentified at the moment and would be a fruitful subject for further study.

Neuropsychological symptoms in patients with RA are reported at a long period from disease onset (44). Various disease models with short temporal activation of the immune system, such as bleomycin-induced lung injury and dextran sulfate sodium induced colitis (26,27), suggest that activation of microglia in the sCVOs accompanies inflammatory symptoms, but only for a limited period. Acute systemic injection of IL-1β, TNF-α, and lipopolysaccharide (LPS) increase c-Fos expression in the AP within a short latency and duration (19,45–47). Use of these acute immune system activators has limitations for addressing the issue of whether chronic auto-immune activation results in sustained activation of brain activities. In this regard, the present study is the first to demonstrate that microglia in the AP remain activated for a prolonged period, more than 80 days after the initial immunization in this long-lasting auto-immune arthritis model. This may explain why neuropsychological complications can be observed as the disease lasts or even the arthritis is mitigated by disease-modifying drugs (48). Indeed, Oto *et al*. have demonstrated that behavioral complications in this CIA model of mice become uncorrelated with arthritis score after improvement of arthritis by tofacitinib (33). It is an important future subject to clarify whether the sustained alterations of AP microglia in this CIA model are reversible after pharmacological intervention.

In this study, in addition to the sustained increase in the number of AP microglia, we observed marked changes in their shape during the establishment-to-chronic phases. It is well established that microglia morphology represents the activated state of these cells. For example, Fernandez-Arjona *et al*. quantitatively analyzed microglial morphology in detail in response to immunological challenges in the cortex, striatum, hippocampus (49), and thalamus (50). They found that microglia cells could be clustered into several morphological categories. To categorize microglial morphology in the AP at different CIA phases, we used a similar PCA strategy as these previous studies, albeit with appropriate modification because: 1) unlike in many other brain structures, microglia in the AP are already mildly activated in healthy conditions (20); 2) unlike in acute inflammation models used previously, long-lasting

systemic inflammation of autoimmune arthritis, as in the CIA model, is likely weaker; and 3) the density of resident microglia is much higher in the AP than in other non-sCVO brain regions, therefore measurement of the number and length of microglial processes is challenging and inaccurate, particularly when the number of microglia is further increased. The significant increase in proportion of “cluster-1 cells” in the complete course of symptomatic phases of CIA suggests that AP microglia cells are continuously activated in CIA mice. In support of this morphological activation of microglia in the AP of CIA model, the number of *IL-1β*-positive microglia (*IL-1β*$^{+}$*Iba-1*$^{+}$DAPI$^{+}$) and proportion of *IL-1 β*$^{high}$*Iba-1*$^{+}$DAPI$^{+}$ to *IL-1β*$^{+}$*Iba-1*$^{+}$DAPI$^{+}$ cells in the AP of CIA mice were significantly increased at the establishment phase. These results are in agreement with a previous report showing an increase in IL-1β expression in microglial cells with progression of morphological activation (50), which suggests that increased AP microglia are also functionally activated in CIA mice.

Limitations of this study include the unidentified cellular origin of the increased microglia in the AP. Immunostaining with Iba-1 is positive not only with microglia of brain origin but also with invading monocytes of peripheral origin (46). It remains a future research subject to determine whether the proportion of microglia of cerebral and peripheral origins varies. Another limitation is that we have not demonstrated a causal relationship between inflammatory humoral factors and microglial activation. Future study will address what humoral factor is critical in microglial activation in the AP of CIA.

# Conclusion

We have demonstrated a sustained increase in the number of microglia accompanied by their morphological activation in the AP during persistent arthritis in a CIA mouse model. It is therefore possible that peripheral inflammation inherent with RA may chronically and directly affect microglia in brain regions lacking a BBB and lead to various neural consequences. Thus, we propose a novel pathway linking arthritis to neuropsychological complications in RA patients.

# Abbreviations

ANOVA: analysis of variance; AP: area postrema; BBB: blood–brain barrier; CFA: complete Freund’s adjuvant; CIA: collagen-induced arthritis; CNS: central nervous system; DAPI: 4',6-diamidino-2-phenylindole; FA: Freund’s adjuvant; FITC: fluorescein isothiocyanate; GFAP: glial fibrillary acidic protein; HCA: hierarchical clustering analysis; Iba-1: ionized calcium-binding adaptor molecule-1; IFA: incomplete Freund’s adjuvant; IFN-γ: interferon-gamma; IL: interleukin; LPS: lipopolysaccharide; OVLT: organum vasculosum laminae terminalis; PB: phosphate buffer; PBS: phosphate-buffered saline; PC-1: first principal component; PC-2: second principal component; PCA: principal component analysis; PCR: polymerase chain reaction; PFA: paraformaldehyde; PID: post-immunization days; RA: rheumatoid arthritis; sCVOs: sensory circumventricular organs; SFO: subfornical organs; TNF: tumor necrosis factor.

# Declarations

# Ethics approval

Manipulation of animals was approved by the Institutional Animal Care and Use Committee of Jikei University (approval number 2018-076). All experiments conformed to the Guidelines for Proper Conduct of Animal Experiments of the Science Council of Japan (2006).

# Consent for publication

Not applicable

# Availability of data and materials

The datasets used and/or analyzed during the current study are available from the corresponding author on reasonable request.

# Competing interests

The authors declare that they have no competing interests.

# Funding

This project was funded by grants from the Ministry of Education, Culture, Sports, Science and Technology (MEXT) Supported Program for the Strategic Research Foundation at Private Universities (No. S1311009 [2013-2019]) to FK, and research grants from the Uehara Memorial Foundation to FK.

# Author’s contributions

The research project was designed by TM, YT and FK. TM, YO, and KO performed the experiments. TM analyzed the data. TM, DK, and FK wrote the manuscript. All authors approved the final version of the manuscript.

# Acknowledgement

We gratefully acknowledgement the technical assistance of Ms. Ying Kaku and Dr. Masayuki Yoshiga. We thank Rachel James, Ph.D., from Edanz Group (https://en-author-services.edanz.com/ac) for editing a draft of this manuscript.

## References

1. Matcham F, Rayner L, Steer S, Hotopf M. The prevalence of depression in rheumatoid arthritis: a systematic review and meta-analysis. Rheumatology. 2013 Dec 1;52(12):2136–48.
2. Meeus M, Vervisch S, De Clerck LS, Moorkens G, Hans G, Nijs J. Central sensitization in patients with rheumatoid arthritis: A systematic literature review. Semin Arthritis Rheum. 2012 Feb;41(4):556–67.
3. Meade T, Manolios N, Cumming SR, Conaghan PG, Katz P. Cognitive Impairment in Rheumatoid Arthritis: A Systematic Review. Arthritis Care Res (Hoboken). 2018 Jan;70(1):39–52.
4. Katz P. Fatigue in Rheumatoid Arthritis. Vol. 19, Current Rheumatology Reports. Current Medicine Group LLC 1; 2017. p. 1–10.
5. Matcham F, Davies R, Hotopf M, Hyrich KL, Norton S, Steer S, et al. The relationship between depression and biologic treatment response in rheumatoid arthritis: An analysis of the British Society for Rheumatology Biologics Register. Rheumatology. 2018 May 1;57(5):835–43.
6. Ang DC, Choi H, Kroenke K, Wolfe F. Comorbid depression is an independent risk factor for mortality in patients with rheumatoid arthritis. J Rheumatol. 2005;32(6).
7. Kojima M, Kojima T, Ishiguro N, Oguchi T, Oba M, Tsuchiya H, et al. Psychosocial factors, disease status, and quality of life in patients with rheumatoid arthritis. J Psychosom Res. 2009 Nov 1;67(5):425–31.
8. Deb A, Dwibedi N, Lemasters T, Hornsby JA, Wei W, Sambamoorthi U. Burden of Depression among Working-Age Adults with Rheumatoid Arthritis. 2018;
9. Schrepf A, Kaplan CM, Ichesco E, Larkin T, Harte SE, Harris RE, et al. A multi-modal MRI study of the central response to inflammation in rheumatoid arthritis. Nat Commun. 2018 Dec 1;9(1):2243.
10. Sisó S, Jeffrey M, González L. Sensory circumventricular organs in health and disease. Acta Neuropathol. 2010 Dec 10;120(6):689–705.
11. Ericsson A, Liu C, Hart RP, Sawchenko PE. Type 1 interleukin-1 receptor in the rat brain: Distribution, regulation, and relationship to sites of IL-1-induced cellular activation. J Comp Neurol. 1995 Oct 30;361(4):681–98.
12. Korim WS, Elsaafien K, Basser JR, Setiadi A, May CN, Yao ST. In renovascular hypertension, TNF-α type-1 receptors in the area postrema mediate increases in cardiac and renal sympathetic nerve activity and blood pressure. Cardiovasc Res. 2018 Oct 25;
13. Vallières L, Rivest S. Regulation of the Genes Encoding Interleukin-6, Its Receptor, and gp130 in the Rat Brain in Response to the Immune Activator Lipopolysaccharide and the Proinflammatory Cytokine Interleukin-1β. J Neurochem. 1997 Oct 1;69(4):1668–83.
14. Robertson B, Kong GY, Peng ZC, Bentivoglio M, Kristensson K. Interferon-γ-responsive neuronal sites in the normal rat brain: Receptor protein distribution and cell activation revealed by Fos induction. Brain Res Bull. 2000 May 1;52(1):61–74.
15. Mennicken F, Chabot J-G, Quirion R. Systemic administration of kainic acid in adult rat stimulates expression of the chemokine receptor CCR5 in the forebrain. Glia. 2002 Feb 1;37(2):124–38.

16. Mohsen Z, Sim H, Garcia-Galiano D, Han X, Bellefontaine N, Saunders TL, et al. Sexually dimorphic distribution of Prokr2 neurons revealed by the Prokr2-Cre mouse model. Brain Struct Funct. 2017 Jun 14;
17. Nadjar A, Combe C, Layé S, Tridon V, Dantzer R, Amédée T, et al. Nuclear factor κB nuclear translocation as a crucial marker of brain response to interleukin-1. A study in rat and interleukin-1 type I deficient mouse. J Neurochem. 2004 Feb 4;87(4):1024–36.
18. Harré E-M, Roth J, Pehl U, Kueth M, Gerstberger R, Hübschle T. Selected Contribution: Role of IL-6 in LPS-induced nuclear STAT3 translocation in sensory circumventricular organs during fever in rats. J Appl Physiol. 2002 Jun 1;92(6):2657–66.
19. Lee HY, Whiteside MB, Herkenham M. Area postrema removal abolishes stimulatory effects of intravenous interleukin-1β on hypothalamic-pituitary-adrenal axis activity and c-fos mRNA in the hypothalamic paraventricular nucleus. Brain Res Bull. 1998 Aug 1;46(6):495–503.
20. Takagi S, Furube E, Nakano Y, Morita M, Miyata S. Microglia are continuously activated in the circumventricular organs of mouse brain. J Neuroimmunol. 2019 Jun 15;331:74–86.
21. Nimmerjahn A, Kirchhoff F, Helmchen F. Resting microglial cells are highly dynamic surveillants of brain parenchyma in vivo. Science (80- ). 2005 May 27;308(5726):1314–8.
22. Walker FR, Beynon SB, Jones KA, Zhao Z, Kongsui R, Cairns M, et al. Dynamic structural remodelling of microglia in health and disease: A review of the models, the signals and the mechanisms. Vol. 37, Brain, Behavior, and Immunity. Academic Press; 2014. p. 1–14.
23. Zhang L, Zhang J, You Z. Switching of the microglial activation phenotype is a possible treatment for depression disorder. Vol. 12, Frontiers in Cellular Neuroscience. Frontiers Media S.A.; 2018.
24. York EM, Bernier L-P, MacVicar BA. Microglial modulation of neuronal activity in the healthy brain. Dev Neurobiol. 2018 Jun 1;78(6):593–603.
25. Davis EJ, Foster TD, Thomas WE. Cellular forms and functions of brain microglia. Vol. 34, Brain Research Bulletin. Elsevier; 1994. p. 73–8.
26. Litvin DG, Denstaedt SJ, Borkowski LF, Nichols NL, Dick TE, Smith CB, et al. Peripheral-to-central immune communication at the area postrema glial-barrier following bleomycin-induced sterile lung injury in adult rats. Brain Behav Immun. 2020 Feb 22;
27. Dempsey E, Abautret-Daly Á, Docherty NG, Medina C, Harkin A. Persistent central inflammation and region specific cellular activation accompany depression- and anxiety-like behaviours during the resolution phase of experimental colitis. Brain Behav Immun. 2019 May 4;
28. Gwon S-Y, Rhee K-J, Sung HJ. Gene and Protein Expression Profiles in a Mouse Model of Collagen-Induced Arthritis. Int J Med Sci. 2018;15(1):77–85.
29. Nakamura Y. Regulating Factors for Microglial Activation. Biol Pharm Bull. 2002 Aug;25(8):945–53.
30. Liu X, Nemeth DP, McKim DB, Zhu L, DiSabato DJ, Berdysz O, et al. Cell-Type-Specific Interleukin 1 Receptor 1 Signaling in the Brain Regulates Distinct Neuroimmune Activities. Immunity. 2019 Jan 22;

31. Streit WJ, Hurley SD, McGraw TS, Semple-Rowland SL. Comparative evaluation of cytokine profiles and reactive gliosis supports a critical role for interleukin-6 in neuron-glia signaling during regeneration. J Neurosci Res. 2000 Jul 1;61(1):10–20.
32. Miyata S, Morita S. A new method for visualization of endothelial cells and extravascular leakage in adult mouse brain using fluorescein isothiocyanate. J Neurosci Methods. 2011 Oct 30;202(1):9–16.
33. Oto Y, Takahashi Y, Kurosaka D, Kato F. Alterations of voluntary behavior in the course of disease progress and pharmacotherapy in mice with collagen-induced arthritis. Arthritis Res Ther. 2019 Dec 12;21(1).
34. Ito H, Noda K, Yoshida K, Otani K, Yoshiga M, Oto Y, et al. Prokineticin 2 antagonist, PKRA7 suppresses arthritis in mice with collagen-induced arthritis. BMC Musculoskelet Disord. 2016 Sep 8;17(1):387.
35. Morita S, Furube E, Mannari T, Okuda H, Tatsumi K, Wanaka A, et al. Heterogeneous vascular permeability and alternative diffusion barrier in sensory circumventricular organs of adult mouse brain. Cell Tissue Res. 2016 Feb 6;363(2):497–511.
36. Kanda Y. Investigation of the freely available easy-to-use software “EZR” for medical statistics. Bone Marrow Transplant. 2013 Mar 3;48(3):452–8.
37. Knoll JG, Krasnow SM, Marks DL. Interleukin-1β signaling in fenestrated capillaries is sufficient to trigger sickness responses in mice. J Neuroinflammation. 2017 Dec 9;14(1):219.
38. Vargas-Caraveo A, Pérez-Ishiwara DG, Martínez-Martínez A. Chronic Psychological Distress as an Inducer of Microglial Activation and Leukocyte Recruitment into the Area Postrema. Neuroimmunomodulation. 2015 Aug 20;22(5):311–21.
39. Brown E, Mc Veigh CJ, Santos L, Gogarty M, Müller HK, Elfving B, et al. TNFα-dependent anhedonia and upregulation of hippocampal serotonin transporter activity in a mouse model of collagen-induced arthritis. Neuropharmacology. 2018 Jul 15;137:211–20.
40. Lee S, Zhao YQ, Ribeiro-da-Silva A, Zhang J. Distinctive response of CNS glial cells in oro-facial pain associated with injury, infection and inflammation. Mol Pain. 2010 Nov 10;6:79.
41. Kim SU, De Vellis J. Microglia in health and disease. Vol. 81, Journal of Neuroscience Research. John Wiley & Sons, Ltd; 2005. p. 302–13.
42. Illes P, Rubini P, Ulrich H, Zhao Y, Tang Y. Regulation of Microglial Functions by Purinergic Mechanisms in the Healthy and Diseased CNS. Vol. 9, Cells. NLM (Medline); 2020.
43. Reis WL, Yi C-X, Gao Y, Tschöp MH, Stern JE. Brain Innate Immunity Regulates Hypothalamic Arcuate Neuronal Activity and Feeding Behavior. Endocrinology. 2015 Apr 1;156(4):1303–15.
44. Hewlett S, Cockshott Z, Byron M, Kitchen K, Tipler S, Pope D, et al. Patients’ perceptions of fatigue in rheumatoid arthritis: Overwhelming, uncontrollable, ignored. Arthritis Care Res. 2005 Oct 15;53(5):697–702.
45. Bernstein IL, Taylor EM, Bentson KL. TNF-induced anorexia and learned food aversions are attenuated by area postrema lesions. Am J Physiol - Regul Integr Comp Physiol. 1991;260(5 29-5).

46. Furube E, Kawai S, Inagaki H, Takagi S, Miyata S. Brain Region-dependent Heterogeneity and Dose-dependent Difference in Transient Microglia Population Increase during Lipopolysaccharide-induced Inflammation. Sci Rep. 2018 Dec 2;8(1):2203.
47. Dallaporta M, Pecchi E, Jacques C, Berenbaum F, Jean A, Thirion S, et al. c-Fos immunoreactivity induced by intraperitoneal LPS administration is reduced in the brain of mice lacking the microsomal prostaglandin E synthase-1 (mPGES-1). Brain Behav Immun. 2007 Nov 1;21(8):1109–21.
48. Ishida M, Kuroiwa Y, Yoshida E, Sato M, Krupa D, Henry N, et al. Residual symptoms and disease burden among patients with rheumatoid arthritis in remission or low disease activity: a systematic literature review. Mod Rheumatol. 2018 Sep 3;28(5):789–99.
49. Soltys Z, Orzylowska-Sliwinska O, Zaremba M, Orlowski D, Piechota M, Fiedorowicz A, et al. Quantitative morphological study of microglial cells in the ischemic rat brain using principal component analysis. J Neurosci Methods. 2005 Jul 15;146(1):50–60.
50. Fernandez-Arjona M, Grondona JM, Fernández-Llebrez P, Lopez-Avalos MD. Microglial morphometric parameters correlate with the expression level of IL-1β, and allow identifying different activated morphotypes. Front Cell Neurosci. 2019;13:472.

# Figures

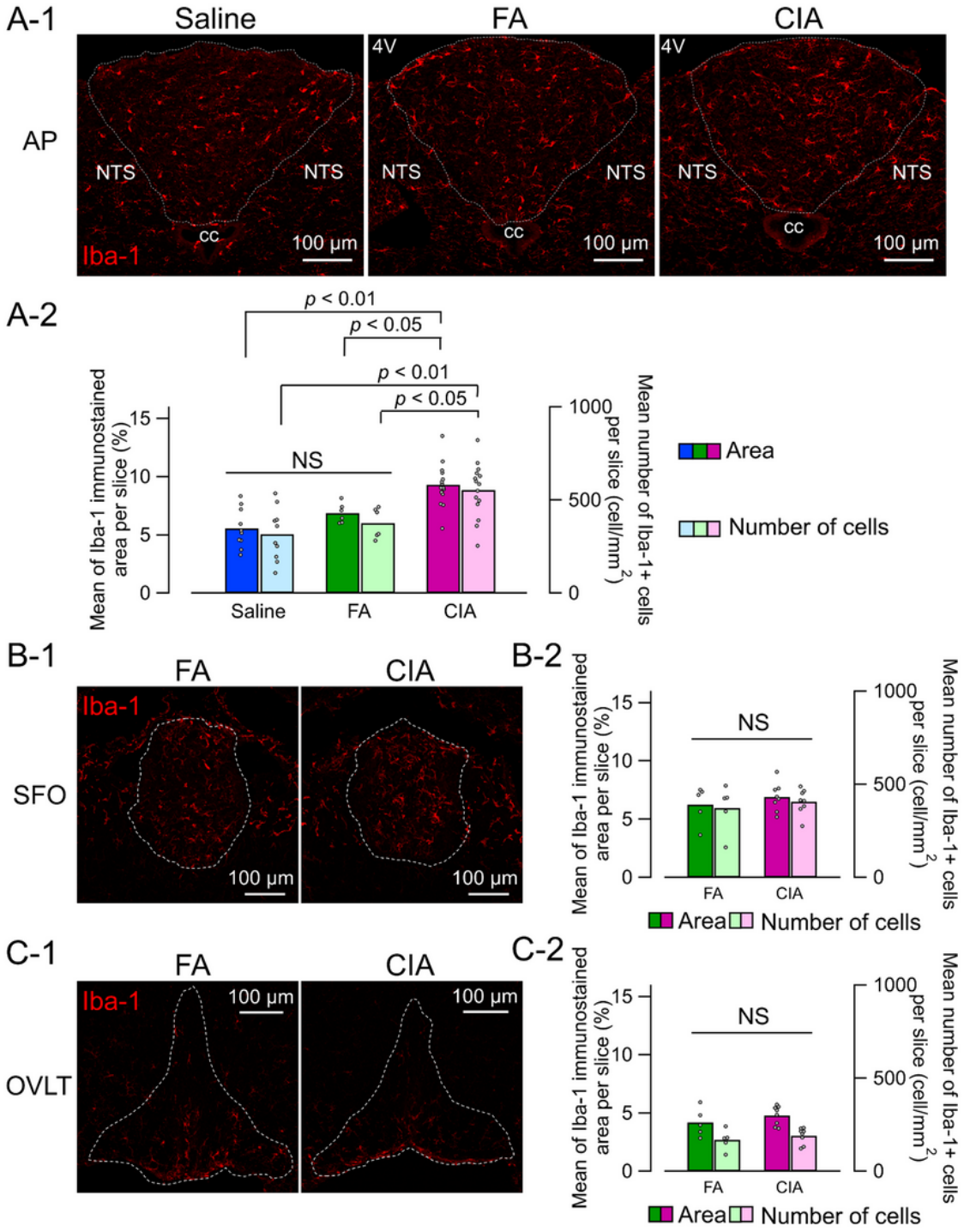


## Figure 1

Microglia in the sensory circumventricular organs of collagen-induced arthritis mouse models on post-immunization day 35. A-1: Representative images of immunostaining for ionized calcium-binding protein-1 (Iba-1) in the area postrema (AP). A-2: Quantitative analysis of Iba-1 immunostained area (%) and number of Iba-1-positive cells in the AP. Iba-1-positive cells were significantly larger in the collagen-induced arthritis (CIA) group (n = 15) compared with the saline (n = 10) and Freund's adjuvant (FA)

groups (n = 6) by one-way analysis of variance with Bonferroni's post-hoc test. There were no significant differences between the saline and FA groups. B-1: Representative images of Iba-1 immunostaining in the subfornical organs (SFO). B-2: Quantitative analysis in the SFO. There were no significant differences between groups by unpaired t-test (CIA, n = 8; FA, n = 5). C-1: Representative images of Iba-1 immunostaining in the organum vasculosum laminae terminalis (OVLT). C-2: Quantitative analysis in the OVLT. There were no significant differences between groups by unpaired t-test (CIA, n = 8; FA, n = 5). Abbreviations: 4V: fourth ventricle; NTS, nucleus of the solitary tract; cc central canal; NS, non-significant.

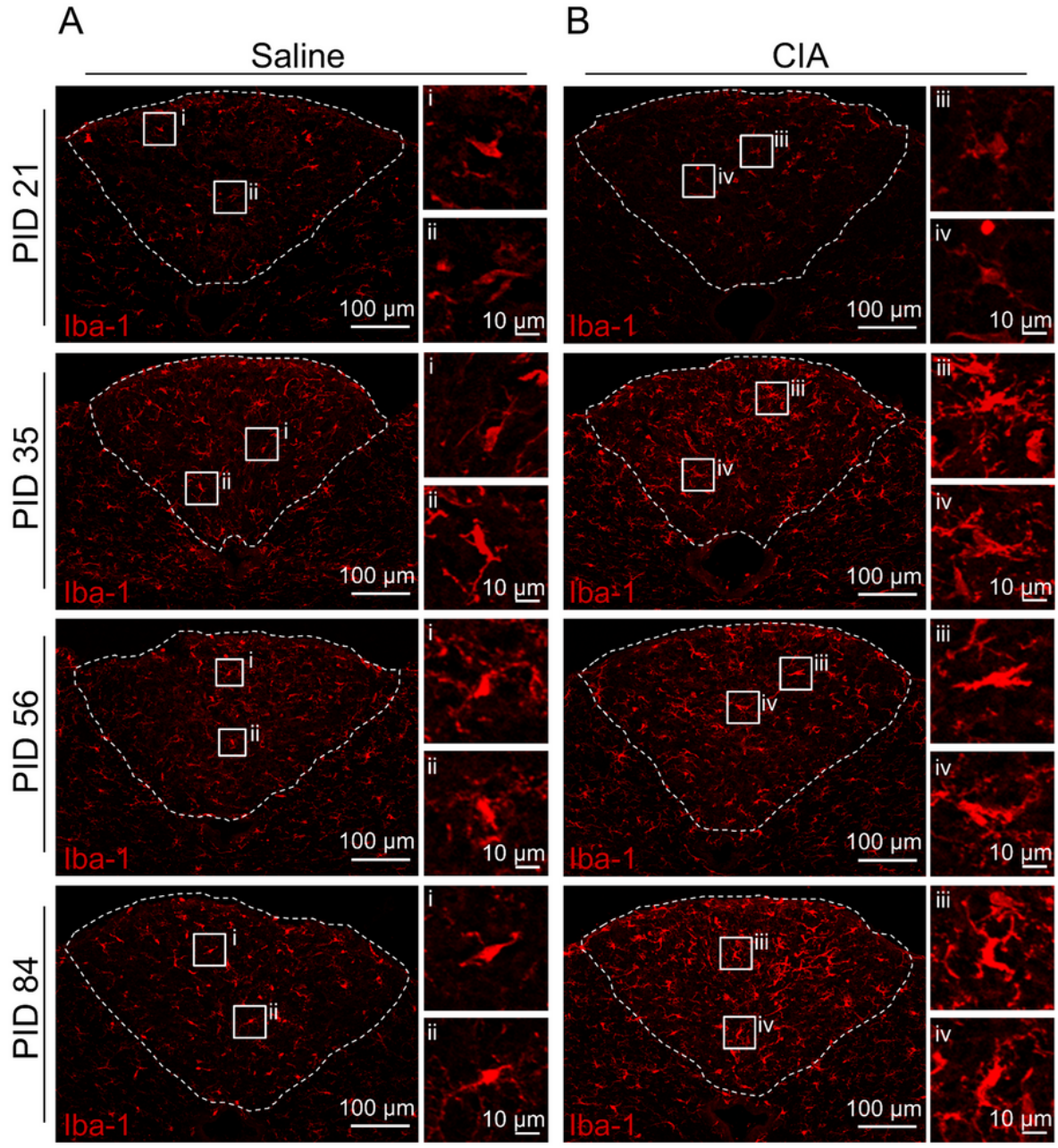

## Figure 2

Immunostaining for ionized calcium-binding adaptor protein-1 in the area postrema by disease phase. A: Representative images in the saline group. Boxed areas are shown at higher magnification on the right (i and ii). B: Representative images in the collagen-induced arthritis (CIA) group. Boxed areas are shown at higher magnification on the right (iii and iv). Abbreviation: PID, post-immunization day.

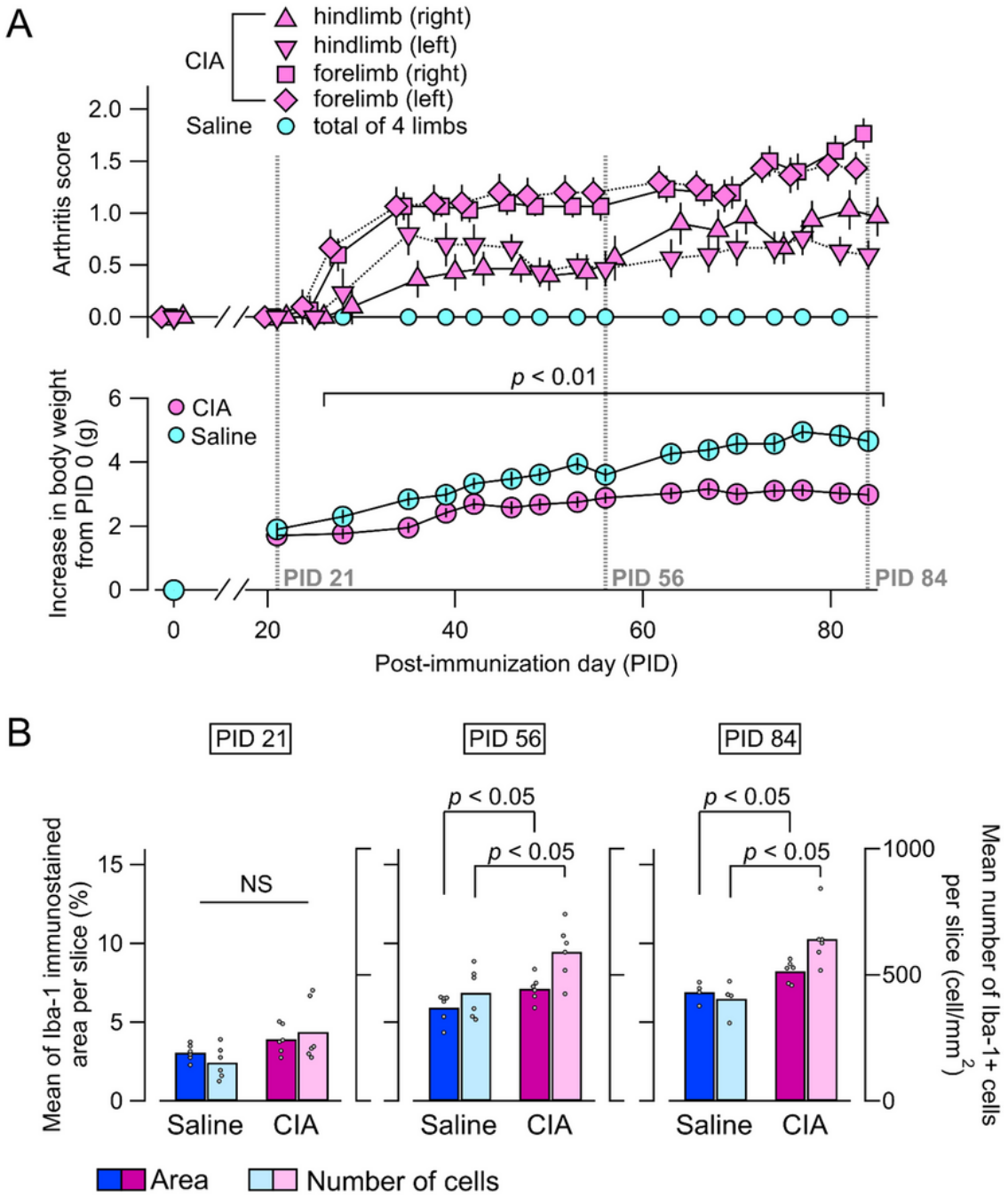


## Figure 3

Arthritis scores, body weight changes, and ionized calcium-binding adaptor protein-1 immunoreactivity by disease phase. A: Time course of arthritis scores (upper panel) and body weight changes (lower panel) (CIA, n = 30; saline, n = 24). The dashed line represents the day of brain analysis. No arthritic mice were found on post-immunization day (PID) 21. Arthritis scores gradually increased after onset. Joint swelling was sustained on PID 84. Body weight changes in the collagen-induced arthritis (CIA) group were significantly lower compared with the saline group after PID 28 (unpaired t-test). B: Quantitative analysis of ionized calcium-binding adaptor protein-1 (Iba-1) immunostained area (%) and number of Iba-1-positive cells. There were no significant differences between groups on PID 21 by unpaired t-test (CIA, n = 6; saline, n = 6). Conversely, area and number were significantly larger in the CIA group compared with the saline group on PID 56 (CIA, n = 6; saline, n = 6) and 84 (CIA, n = 6; saline, n = 4) by unpaired t-test. Abbreviation: NS, non-significant.

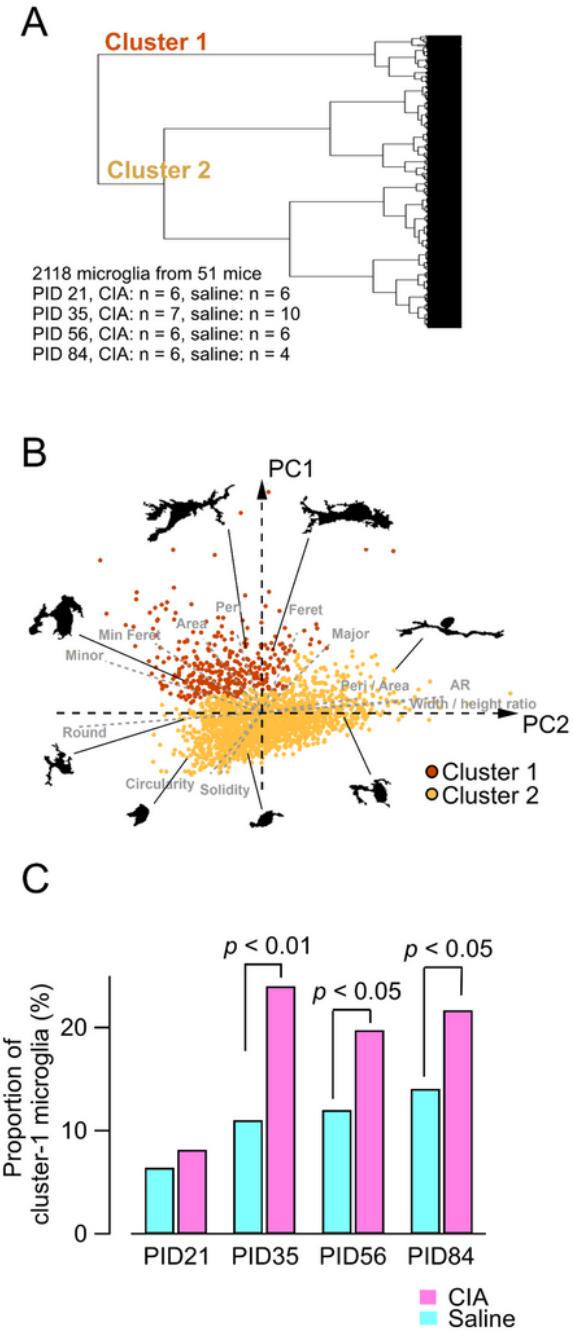


## Figure 4

Morphological classification of microglia and increase of the activated form cluster during arthritis. A: Dendrogram by hierarchical clustering analysis using the first two principal components (PC-1 and PC-2). Microglia were classified into cluster-1 and cluster-2. B: Morphological plots of each cluster on PC-1 and PC-2 coordinate planes with examples of their morphology. Gray dashed lines reflect loading plots. C: Proportion of cluster-1 microglia in each disease phase. There were no differences between groups on

post-immunization day (PID) 21 by chi-squared test. Conversely, the proportion in the collagen-induced arthritis (CIA) group was higher than the saline groups on PID 35, 56, and 84 by chi-squared test. Abbreviations: Peri, perimeter; Min Feret, minimum Ferret diameter; Minor, minor diameter; Round, roundness; AR, aspect ratio; Peri/Area, ratio of perimeter to area; Major, major diameter; Feret, Feret diameter.

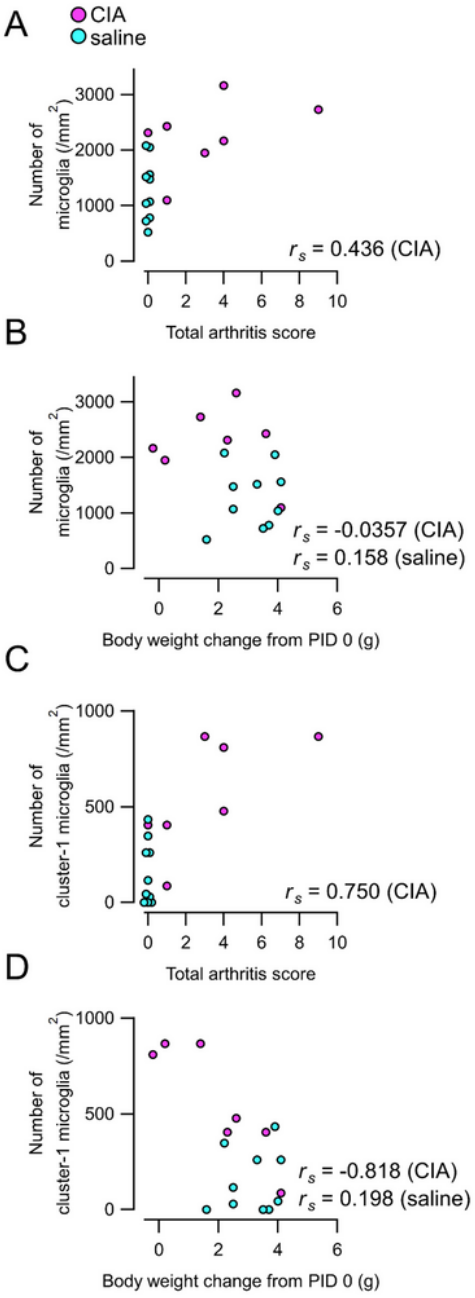


**Figure 5**

Correlation of microglia number with total arthritis scores and body weight changes. A, B: Correlation of total microglia number with total arthritis scores (A) and body weight changes from PID 0 (B). C, D: Correlation of number of cluster-1 microglia with total arthritis scores (C) and body weight changes (D). The number of cluster-1 microglia significantly correlated with body weight changes (rs = -0.818, n = 7, p = 0.0244; Spearman rank correlation coefficient). Abbreviations: CIA, collagen-induced arthritis; PID, post-immunization day.

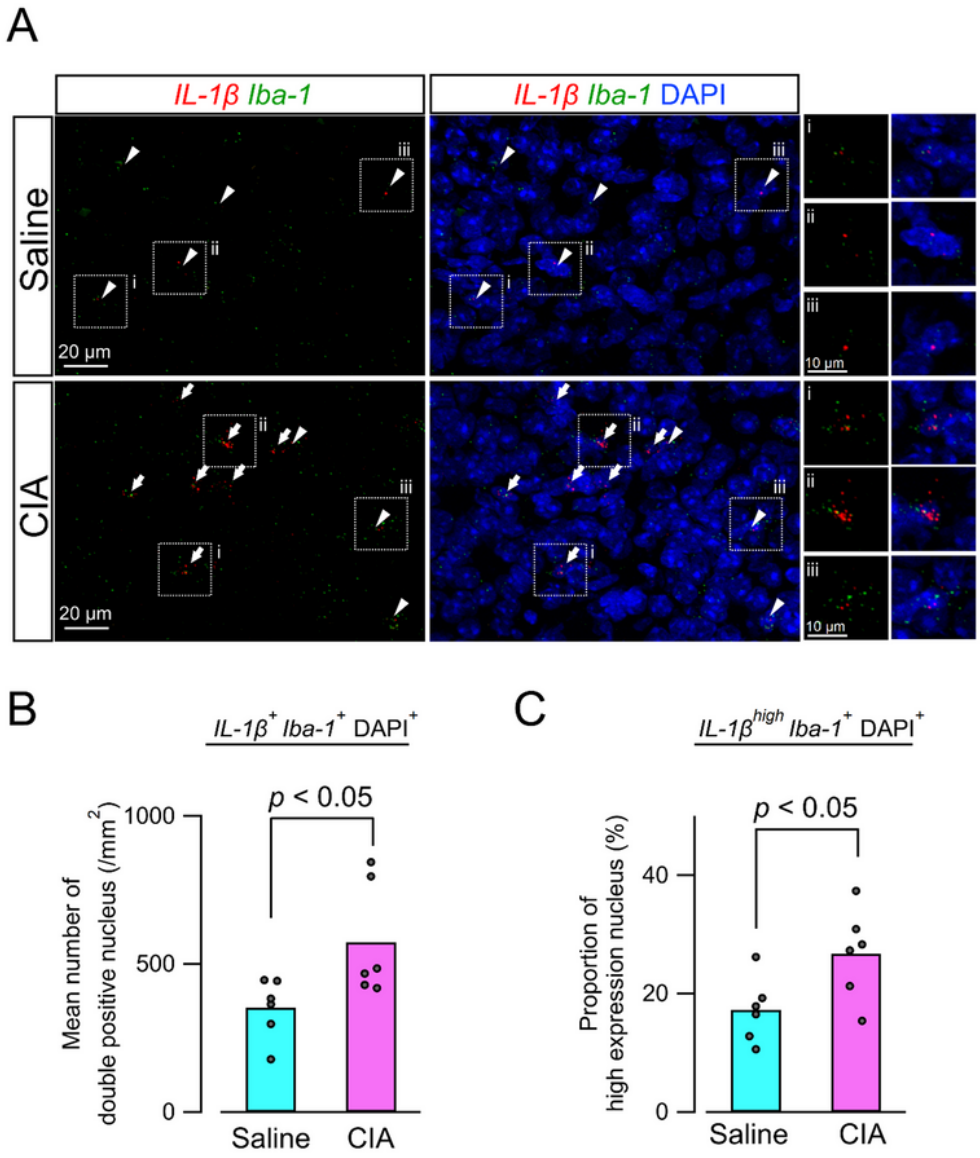


**Figure 6**

Microglial interleukin-1β mRNA expression in the area postrema. A: Representative merged images of interleukin-1β (IL-1β) (red) and ionized calcium-binding adaptor protein-1 (Iba-1) (green) mRNA expression in the area postrema (AP). Boxed areas are shown at higher magnification on the right (i, ii, and iii). Arrowheads indicate nuclei (DAPI, blue) co-expressing IL-1β mRNA and Iba-1 mRNA. Arrows indicate Iba-1-postive nuclei with high-density expression of IL-1β mRNA (four or more nuclear puncta). In the collagen-induced arthritis (CIA) group, more nuclei co-expressing IL-1β and Iba-1 were observed. Additionally, Iba-1-postive nuclei with high-density expression of IL-1β mRNA were more frequently detected in the CIA group. B: Quantitative analysis of the number of nuclei co-expressing IL-1β and Iba-1. In the CIA group (n = 6), these nuclei were significantly increased compared with the saline group (n = 6) by unpaired t-test. C: Quantitative analysis of the proportion of Iba-1-postive nuclei with high-density expression of IL-1β mRNA. The proportion significantly increased in the CIA group (CIA, n = 6; saline, n = 6) by unpaired t-test.

## Supplementary Files

This is a list of supplementary files associated with this preprint. Click to download.

- SupplementaryFigure1.tif
- SupplementaryFigure2.tif
- SupplementaryFigure3.tif
- SupplementaryFigure4.tif
- SupplementaryFigure5.tif
- SupplementaryFigure6.tif
- SupplementaryFigure7.tif
- SupplementaryFigure8.tif
- Supplementaryfigurelegends.docx